Available online at www.sciencedirect.com

ScienceDirect

journal homepage: www.elsevier.com/locate/he

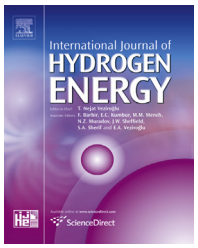

# Gas and vapor adsorption in octacyanometallate-based frameworks $Mn_2[M(CN)_8]$ (M = W, Mo) with exposed $Mn^{2+}$ sites

*Aihua Yuan* [a,*], *Hu Zhou* [a,b], *Guowang Diao* [b], *Peter D. Southon* [c], *Cameron J. Kepert* [c,**], *Lang Liu* [d]

[a] *School of Biology and Chemical Engineering, Jiangsu University of Science and Technology, Zhenjiang 212003, China*

[b] *School of Chemistry and Chemical Engineering, Yangzhou University, Yangzhou 225002, China*

[c] *School of Chemistry, University of Sydney, Sydney 2006, Australia*

[d] *Institute of Applied Chemistry, Xinjiang University, Urumqi 830046, China*

ARTICLE INFO

*Article history:*
Received 15 June 2013
Received in revised form
16 October 2013
Accepted 25 October 2013
Available online 18 November 2013

*Keywords:*
Octacyanometallates
Porous
Adsorption
Enthalpy

ABSTRACT

Dehydration of the isostructural three-dimensional (3D) octacyanometallate-based materials $Mn_2M(CN)_8 \cdot 7H_2O$ (M = Mo, **1·7H$_2$O**; W, **2·7H$_2$O**) generates robust porous frameworks (**1** and **2**). In the structure, the $[M(CN)_8]^{4-}$ units are linked *via* octahedral $Mn^{2+}$ centers to form an open 3D framework with 1D channels, in which the non-coordinated and coordinated water molecules are involved. The permanent porosities have been confirmed by thermogravimetric analysis, variable-temperature X-ray diffraction and Raman spectra, and adsorption ($H_2O$, $N_2$ and $H_2$) measurements. $H_2$ adsorption at 1.1 bar and 77 K was 0.60 wt% for **1** and 0.49 wt% for **2**. At initial loading $\Delta H_{ads}$ has the value of *ca.* 10.0 kJ mol$^{-1}$ for both materials, which represents the highest value reported for any cyanide-based assemblies. The high enthalpy can be attributed to the presence of coordinatively-unsaturated $Mn^{2+}$ sites left exposed by the removal of coordinated water molecules in the structure.



## 1. Introduction

Porous coordination frameworks have attracted much attention due to their high permanent porosity, exceptional structural and chemical tunability, and convenient modular synthesis [1–4]. Cyanide-based materials, especially porous Prussian blue analogs, have recently received particular attention in the area of hydrogen storage, owing to their chemical stability, small pores and resulting high volumetric storage densities, and their high density of exposed metal sites [5–8]; such sites have been shown to provide a novel mean for increasing the hydrogen physisorption enthalpy to favor hydrogen loading at non-extreme temperatures and pressures [9–11].

Recently, octacyanometallates $[M(CN)_8]^{3-/4-}$ (M = Mo, W) or $[Nb(CN)]^{4-}$ have been found to be versatile building blocks

* *Corresponding author*. Tel.: +86 511 85638920.
** *Corresponding author*.
E-mail addresses: aihuayuan@163.com (A. Yuan), c.kepert@chem.usyd.edu.au (C.J. Kepert).

0360-3199/$ – see front matter Copyright © 2013, Hydrogen Energy Publications, LLC. Published by Elsevier Ltd. All rights reserved.
http://dx.doi.org/10.1016/j.ijhydene.2013.10.143

and investigated extensively [12,13]. These species can form various geometrical structures, and their flexibilities may assist in the formation of a variety of three-dimensional (3D) open frameworks [14–17]. However, despite the first examples of octacyanometallate-based assemblies, $M_2[Mo(CN)_8]\cdot nH_2O$ ($n = 2–9$) (M = Mn, Fe, Co, Ni, Cu, Zn) having been documented as far back as 1973 [18], relatively few studies have reported their porous properties [19,20], in comparison to the better known Prussian blue analogs. Moreover, it is worth noting that, to the best of our knowledge, the hydrogen gas and vapor adsorption properties of octacyanometallate-based frameworks have remained unexplored.

As a further probe of the role of coordinatively-unsaturated metal centers in the $H_2$ uptake within cyanide-based materials, we report in this contribution the water, nitrogen, and hydrogen adsorption studies of the dehydrated frameworks $Mn_2M(CN)_8$ (M = Mo, **1**; W, **2**) with exposed $Mn^{2+}$ sites.

## 2. Experimental

Unless otherwise mentioned, all reactants were used as purchased, without further purification. A small glass vial (2 mL) containing the solid of $K_4[M(CN)_8]\cdot 2H_2O$ (M = Mo, W) [21,22] (0.15 mmol) was placed into a big glass vial (20 mL) containing the solid of $MnCl_2\cdot 2H_2O$ (0.30 mmol). The distilled water was poured slowly into above two vials till the liquid level was just over the small vial. Then the isopropyl alcohol was carefully layered on above solution, and then the big vial was sealed. Slow diffusion of the solutions resulted in yellow needle crystalline samples of $MnMo(CN)_8\cdot 7H_2O$ (**1·7H$_2$O**) and $MnW(CN)_8\cdot 7H_2O$ (**2·7H$_2$O**) after about 2 weeks. The samples were filtered, washed in water and dried in air. X-ray diffraction patterns of as-synthesized products were fully consistent with those simulated from the single-crystal X-ray diffraction data reported previously in the literature [23,24] (Fig. S1, Supplementary information).

Thermal analyses were carried out at a ramp rate of 5 °C $min^{-1}$ under a dry $N_2$ atmosphere using a Pyris Diamond TGA analyzer. Powder X-ray diffraction patterns were collected with $CuK_\alpha$ radiation using a Shimadzu XRD 6000 diffractometer equipped with Anton-Paar HTK 1200 stage for atmosphere and temperature control. Dehydration measurements were run under flowing dry dinitrogen with a heating rate of 1 °C $min^{-1}$. For rehydration measurements, the dinitrogen flow was saturated with water vapor by diverting the flow through a water bubbler. Temperature-dependent Raman spectra were recorded in backscattering geometry using JY-T6400 tripe monochromator. The 785 nm light from an $Ar^+$ laser was focused onto the sample surface under nitrogen atmosphere. The temperature stability of the sample was controlled within 0.1 °C (THMS600/HFS91). The scattered signal from the sample was detected by a charge-coupled device detection system.

Synchrotron powder X-ray diffraction patterns were collected at the Advanced Photon Source at Argonne National Laboratory, 12-BM ($\lambda = 0.61992$ Å) using a MAR-3450 imaging plate detector. The sample was contained in a polyimide capillary with a flowing helium atmosphere, and the temperature was controlled using an Oxford Cryosystems cryostat ramping from 250 to 500 K at 2 K $min^{-1}$. Raw images were processed using Fit-2D. The sample-to-detector distance and tilt of the image plate relative to the beam were refined using a $LaB_6$ standard.

Water adsorption/desorption isotherms were measured using an IGA 002 adsorption instrument (Hiden-Isochema, UK). Sample preparation involved dehydrations of **1·7H$_2$O** and **2·7H$_2$O** under high dynamic vacuum ($<10^{-5}$ mbar) with heating at 100 °C for 12 h, after which the rate of mass loss was negligible (<0.001 wt% $h^{-1}$). During the isotherm measurement the temperature of the sample was maintained at 40 ± 0.1 °C. The sample chamber was pressurized to set pressures of the adsorbent with a ramp time of 120 s, then the pressure and temperature kept constant while the mass was recorded until the equilibration was reached.

Low- and high-pressure gas adsorption measurements were performed on ASAP 2020 and 2050 volumetric instruments supplied by Micromeritics Instruments Inc, respectively. Samples of a known weight (*ca.* 200 mg) were loaded into the glass analysis tube and evacuated at high vacuum for 24 h, then heated at 2 °C $min^{-1}$–150 °C and evacuated for a further 24 h until the outgas rate was less than 3 μbar $min^{-1}$. The sample was then backfilled with $N_2$ before being transferred to the analysis port where it was evacuated for at least a further 4 h before the analysis was started. UHP grade $N_2$ and $H_2$ (99.999%) gases were used for all measurements.

The enthalpy of adsorption ($\Delta H_{ads}$) was obtained by the isosteric method from isotherms recorded at $N_2$ (77 K) and Ar (87 K) baths, and then using the Clausius–Clapeyron equation (1) [25]:

$$\ln\left(\frac{P_1}{P_2}\right) = \frac{\Delta H_{ads}}{R} \times \frac{T_2 - T_1}{T_1 \times T_2} \quad (1)$$

where $P_n$ is the pressure for isotherm $n$ at which a given quantity has been adsorbed, $T_n$ is the temperature for isotherm $n$, and $R$ is the molar gas constant.

Pressure as a function of the quantity of gas adsorbed was calculated by fitting each isotherm using the Langmuir–-Freundlich equation [26]:

$$\frac{Q}{Q_m} = \frac{B \times P^{(1/t)}}{1 + B \times P^{(1/t)}} \quad (2)$$

where Q is the number of moles of gas adsorbed, $Q_m$ the number of moles of gas adsorbed at saturation, $P$ the pressure, and B and t are the fitting constants. Eq. (2) was then substituted into Eq. (1) to give enthalpy of adsorption as function of the quantity of $H_2$ adsorbed.

## 3. Results and discussion

### 3.1. Crystal structures of 1·7H$_2$O and 2·7H$_2$O

The crystal structures of hydrated phases **1·7H$_2$O** and **2·7H$_2$O** are well documented [23,24]. Single-crystal X-ray diffraction revealed that the two compounds are isostructural, and $[M(CN)_8]^{4-}$ units are linked *via* octahedral $Mn^{2+}$ centers to form a porous 3D framework with 1D channels along the *a*

axis, in which coordinated and non-coordinated water molecules are trapped (Fig. 1(a)). The robust nature of the framework enables the rectangle pore windows with the size of approximately 5.0 Å × 3.6 Å to be retained in the absence of non-coordinated and coordinated water molecules, leaving available coordinatively-unsaturated $Mn^{2+}$ sites (Fig. 1(b)).

### 3.2. *Dehydration and rehydration studies*

Thermogravimetric analysis (Fig. 2) of **1·7H$_2$O** and **2·7H$_2$O** revealed that there were three well-pronounced weight-loss steps as the temperature was increased. The first mass loss at *ca.* 60 °C and the second mass loss at *ca.* 120 °C correspond to the loss of three crystallized and four coordinated water molecules per formula unit involved in the pores, leading to the phases **1·4H$_2$O** (or **2·4H$_2$O**) and **1** (or **2**), respectively. The

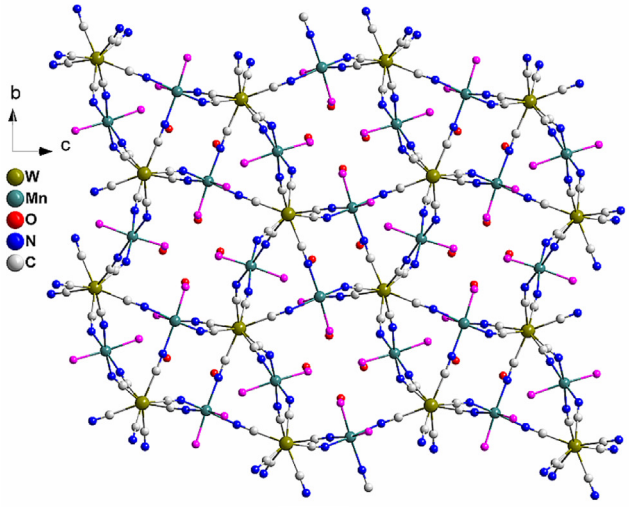


(*a*)

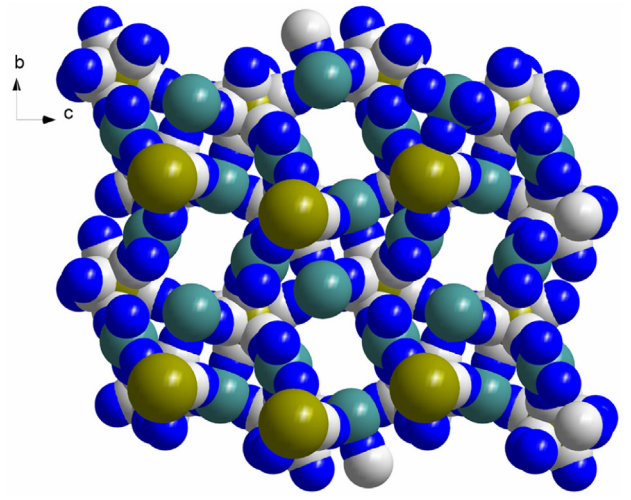


(*b*)

**Fig. 1 – (a) The ball-and-stick structure of 2·7H$_2$O, and (b) the space-filling structure of 2. All hydrogen atoms are omitted for clarity.**

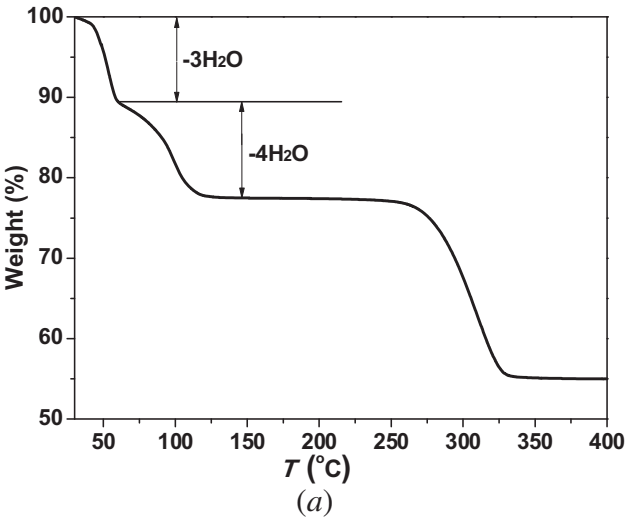


(*a*)

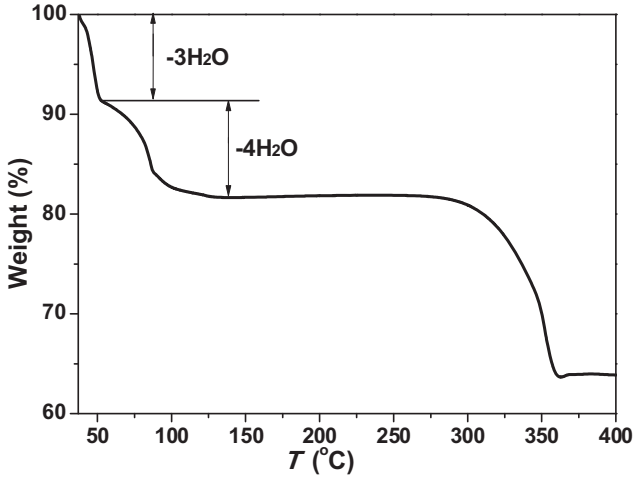


(*b*)

**Fig. 2 – Thermogravimetric curves of (a) 1·7H$_2$O, and (b) 2·7H$_2$O.**

third mass loss above high temperatures is attributed to the thermal decomposition of the host framework.

Variable-temperature and synchrotron powder X-ray diffraction results showed that the structure of both materials changed following the loss of crystallized and coordinated water molecules, with the variable change in the diffraction peaks (Fig. 3, Figs. S2 and S3). The changes in X-ray diffraction patterns are not reversed when cooled to 30 °C under dinitrogen saturated with water vapor. However, the patterns of samples soaked in water are well in accordance with those of hydrated phases **1·4H$_2$O** (or **2·4H$_2$O**), which indicated that the whole dehydration/rehydration process was reversible with slow resorption kinetics. Meanwhile, above results also mean that three crystallized water molecules are more difficult to re-adsorb into the pores than four coordinated water molecules. In addition, the CN stretch derived from variable-temperature Raman spectra for dehydrated phases are shifted toward higher frequencies from those of the hydrated phases, which can be attributed to the fact that the coordination number of Mn(II) center decreases upon heating (Fig. S4).

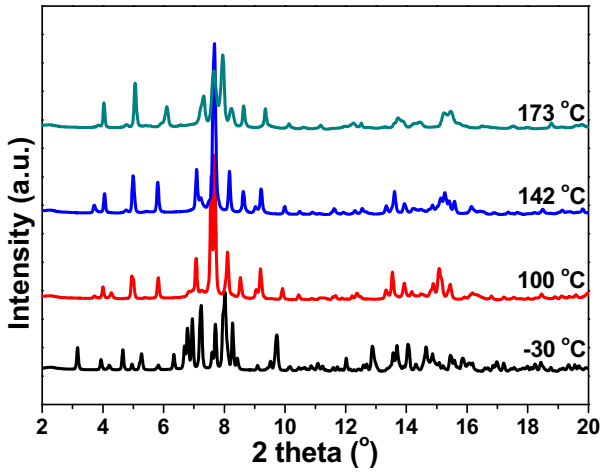


**Fig. 3 – Synchrotron powder X-ray diffraction patterns of $1{\cdot}7H_2O$.**

The water adsorption isotherms of **1** and **2** are shown in Fig. 4, which showed three steps. Three coordinated water molecules per formula unit are readily adsorbed into the pores by $P/P_0 = 0.01$ and a further uptake of one coordinated water molecule is observed at $P/P_0 = 0.2$, corresponding to the transition of 4-coordinated (unsaturated Mn center) to 6-coordinated Mn. The abrupt uptake behavior at low relative pressures is characteristic of strong $H_2O$–$Mn^{2+}$ interaction, since the pores are decorated with coordinatively-unsaturated Mn centers and the water molecule is expected to coordinate to Mn upon its introduction into the pores. However, the origin of the second step, corresponding to the fourth and final coordinated water molecule, is not clear. A third step is observed over the pressure range $P/P_0 = 0.5$–$0.7$, corresponding to the adsorption of an additional three non-coordinated water molecules. Over this range the kinetics of adsorption are very slow and the equilibrium mass could not be extrapolated after a period of over three hours per point; therefore the corresponding points are omitted from the presented isotherm. Extremely slow kinetics would be associated with very narrow pores, or gradual changes in the crystal structure. Unfortunately, further *in-situ* structural studies to elucidate the nature of these steps were not possible, as the single crystals fractured during the dehydration process.

Significant hysteresis was observed between the adsorption and desorption arms of the isotherm, suggestive of energy differences associated with framework structural transformation, which is in accordance with temperature-dependence X-ray diffraction and Raman spectra. The desorption arm also contains two steps, consistent with the TGA results.

### 3.3. *Adsorption of nitrogen and hydrogen*

The nitrogen adsorption data at 1 bar and 77 K for **1** and **2** reveal the type I isotherms (Fig. 5), with BET surface areas of 146(**1**) and 112(**2**) $m^2\ g^{-1}$. The BJH adsorption cumulative volumes of pores for **1** and **2** are 0.027 and 0.020 $cm^3\ g^{-1}$, respectively. At higher pressures a small additional amount is adsorbed, most probably multilayers on the external surface. The surface areas observed for **1** and **2** are significantly lower than those obtained for dehydrated variants of compounds $A_2Zn_3[Fe(CN)_6]_2$ (A = H, Li, Na, K, Rb) [27] and vacancy-riddled Prussian blue analogs of the type $M_3[Co(CN)_6]_2$ (M = Mn, Fe, Co, Ni, Cu, Zn) [7], owing to the difference in framework structures.

The hydrogen adsorption isotherms of **1** and **2** are shown in Fig. 6. Hydrogen adsorption at 1.1 bar and 77 K was 0.60 wt% for **1** and 0.49 wt% for **2**. The trend in hydrogen adsorption correlates well with micropore volumes extracted from nitrogen adsorption data. Assuming only negligible reductions in unit cell volumes as a result of dehydration, this gives minimum volumetric $H_2$ storage densities of 11.36 g $L^{-1}$ for **1** and 10.98 g $L^{-1}$ for **2** at 1.1 bar and 77 K. Obviously, the gravimetric $H_2$ adsorption and the volumetric densities are apparently lower than those reported for most metal-organic and cyanide-based frameworks under comparable conditions [28]. However, the hydrogen adsorption isotherms of both materials exhibit a steep initial rise, signaling a strong interaction between $H_2$ and the host framework. This enhancement may be due to some interaction of the adsorbed $H_2$ with the 4-coordinated Mn sites. Fits to the isotherms with the

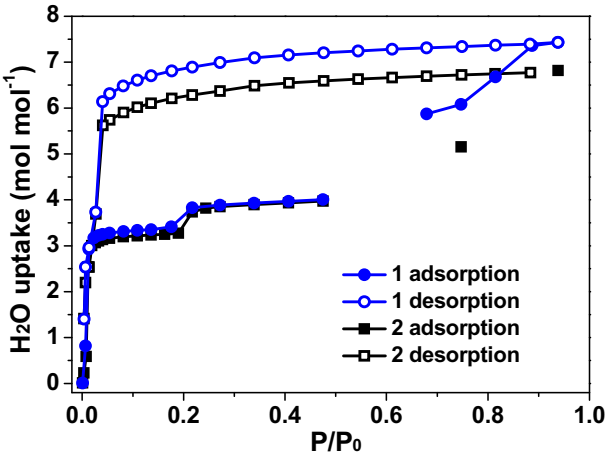


**Fig. 4 – $H_2O$ adsorption and desorption isotherms for 1 and 2.**

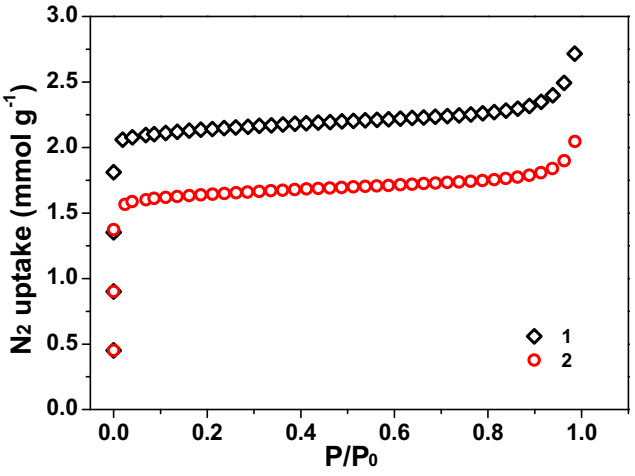


**Fig. 5 – $N_2$ adsorption isotherms for 1 and 2 at 77 K.**

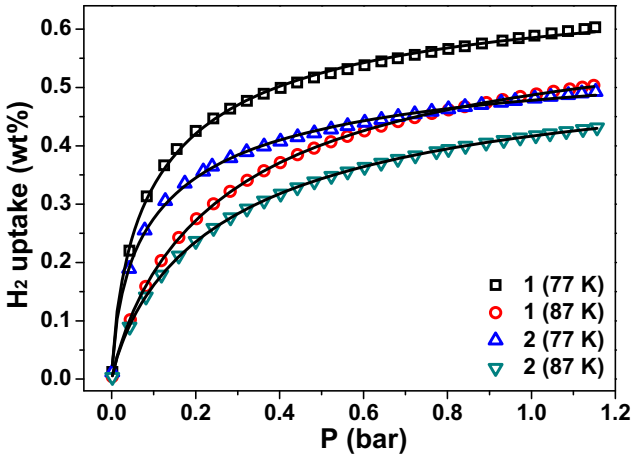


**Fig. 6 – Low-pressure $H_2$ adsorption isotherms for 1 and 2 at 77 K and 87 K, respectively. The solid lines represent the best fit to the data using the Langmuir–Freundlich equation.**

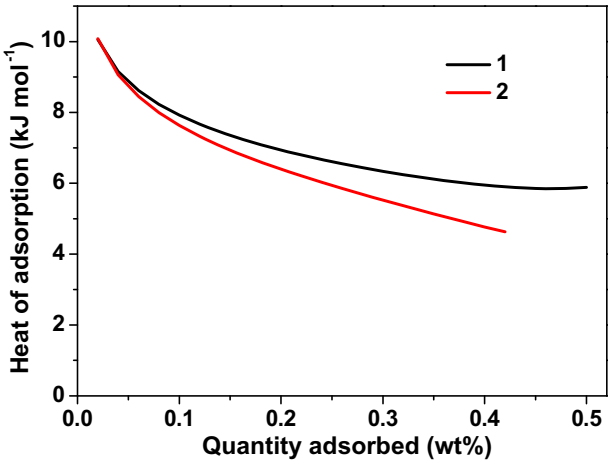


**Fig. 8 – Enthalpy of $H_2$ adsorption for 1 and 2.**

Langmuir–Freundlich equation yielded estimated limiting adsorption capacities of 0.71 wt% for **1**, and 0.59 wt% for **2**, compared to the highest predicted saturation capacity of 2.3 wt% in $Cu_2[Fe(CN)_6]$ for any measured Prussian blue analogs [29]. High-pressure gas adsorption results showed that both dehydrated phases have about 2.56(**1**) and 1.78(**2**) wt% hydrogen uptakes at 10 bar and 77 K (Fig. 7).

The strength of the interaction with the host framework was probed by measuring a second hydrogen adsorption isotherm for each compound at 87 K. Taking both the 77 and 87 K data, a variant of the Clausius–Clapeyron equation was then used to calculate the enthalpy ($\Delta H_{ads}$) of adsorption as a function of the quantity of hydrogen adsorbed (Fig. 8). At initial loading $\Delta H_{ads}$ has the values of 10.06 kJ $mol^{-1}$ for **1** and 10.08 kJ $mol^{-1}$ for **2**, which are within the rather broad range seen for previous cases of $H_2$ binding at bare metal sites, from 6.6 kJ $mol^{-1}$ for $Cu_3[BTC]_2$ [30] to 12.3 kJ $mol^{-1}$ for the recently reported $Zn_3(BDC)_3[Cu(Pyen)]$ [31]. We see that the initial enthalpy observed in this study is higher than that reported for well-known Prussian blue analogs $M_3[Co(CN)_6]_2$ (M = Mn, Fe, Co, Ni, Cu, Zn) (5.9–7.4 kJ $mol^{-1}$) [7] and pillar-layered solids M(L)[M′$(CN)_4$] (M = Co or Ni; L = pillar ligands; M′ = Ni, Pd, or Pd) (6.0–7.8 kJ $mol^{-1}$) [32]. To our knowledge, this represents the highest value reported for any cyanide-based materials. The most energetically favored sites are likely the coordinatively-unsaturated Mn sites left exposed by the removal of coordinated water molecules in the structure.

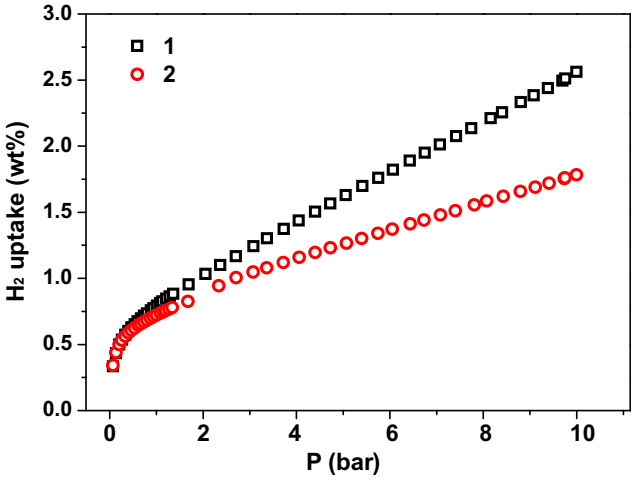


**Fig. 7 – High-pressure $H_2$ adsorption isotherms for 1 and 2 at 77 K.**

## 4. Conclusions

The host–guest interactions and adsorption properties of the isostructural octacyanometallate-based frameworks $Mn_2M(CN)_8$ (M = Mo, W) have been explored. Both materials exhibit permanent porosity and high enthalpy. Significantly, the presence of exposed $Mn^{2+}$ sites in the structure has played an important role in the enhancement of hydrogen binding interaction. Future work will include the use of neutron diffraction methods in studying the $Mn^{2+}$–$H_2$ interactions, and vary the type of metal ions to explore systemically the permanent porosities of related octacyanometallate-based frameworks.

## Acknowledgments

The work is supported by the National Natural Science Foundation of China (51072072, 51102119, 51272095), Natural Science Foundation of Jiangsu Province of China (BK2011518).

## Appendix A. Supplementary information

Supplementary data related to this article can be found at http://dx.doi.org/10.1016/j.ijhydene.2013.10.143.

## REFERENCES


[1] Stock N, Biswas S. Synthesis of metal-organic frameworks (MOFs): routes to various MOF topologies, morphologies, and composites. Chem Rev 2012;112:933–69.

[2] Xuan WM, Zhu CF, Liu Y, Cui Y. Mesoporous metal-organic framework materials. Chem Soc Rev 2012;41:1677–95.

[3] Li JR, Ma YG, McCarthy MC, Sculley J, Yu JM, Jeong HK, et al. Carbon dioxide capture-related gas adsorption and separation in metal-organic frameworks. Coord Chem Rev 2011;255:1791–823.

[4] Meek ST, Greathouse JA, Allendorf MD. Metal-organic frameworks: a rapidly growing class of versatile nanoporous materials. Adv Mater 2011;23:249–67.

[5] Krap CP, Balmaseda J, Zamora B, Reguera E. Hydrogen storage in the iron series of porous Prussian blue analogues. Int J Hydrogen Energy 2010;35:10381–6.

[6] Yuan AH, Chu CX, Zhou H, Yuan P, Liu KK, Li L, et al. Syntheses, crystal structures and gas sorption properties of Prussian blue analogues constructed from $Cr(CN)_6^{3-}$ building blocks. Eur J Inorg Chem 2010:866–71.

[7] Kaye SS, Long JR. Hydrogen storage in the dehydrated Prussian blue analogues $M_3[Co(CN)_6]_2$ (M = Mn, Fe, Co, Ni, Cu, Zn). J Am Chem Soc 2005;127:6506–7.

[8] Chapman KW, Southon PD, Weeks CL, Kepert CJ. Reversible hydrogen gas uptake in nanoporous Prussian blue analogues. Chem Commun 2005:3322–4.

[9] Sumida K, Her JH, Dincă M, Murray LJ, Schloss JM, Pierce CJ, et al. Neutron scattering and spectroscopic studies of hydrogen adsorption in $Cr_3(BTC)_2$-a metal-organic framework. J Phys Chem C 2011;115:8414–21.

[10] Dincă M, Long JR. Hydrogen storage in microporous metal-organic frameworks with exposed metal sites. Angew Chem Int Ed 2008;47:6766–79.

[11] Peterson VK, Liu Y, Brown CM, Kepert CJ. Neutron powder diffraction study of $D_2$ sorption in $Cu_3$(1,3,5-benzenetricarboxylate)$_2$. J Am Chem Soc 2006;128:15578–9.

[12] Nowicka B, Korzeniak T, Stefańczyk O, Pinkowicz D, Chorąży S, Podgajny R, et al. The impact of ligands upon topology and functionality of octacyanidometallate-based assemblies. Coord Chem Rev 2012;256:1946–71.

[13] Sieklucka B, Podgajny R, Korzeniak T, Nowicka B, Pinkowicz D, Kozieł M. A decade of octacyanides in polynuclear molecular materials. Eur J Inorg Chem 2011:305–26.

[14] Nowicka B, Bałanda M, Reczyński M, Majcher AM, Kozieł M, Nitek W, et al. A water sensitive ferromagnetic $[Ni(cyclam)]_2[Nb(CN)_8]$ network. Dalton Trans 2013;42:2616–21.

[15] Pinkowicz D, Rams M, Nitek W, Czarnecki B, Sieklucka B. Evidence for magnetic anisotropy of $[Nb^{IV}(CN)_8]^{4-}$ in a pillared-layered $Mn_2Nb$ framework showing spin-flop transition. Chem Commun 2012;48:8323–5.

[16] Zhou H, Diao GW, Qian SY, Yang XZ, Yuan AH, Song Y, et al. Lanthanide-ion-tuned magnetic properties in a series of three-dimensional cyano-bridged Ln(III)W(V) assemblies. Dalton Trans 2012;41:10690–7.

[17] Zhou H, Yuan AH, Qian SY, Song Y, Diao GW. Efficient synthetic strategy to construct three-dimensional 4f-5d networks using neutral two-dimensional layers as building blocks. Inorg Chem 2010;49:5971–6.

[18] McKnight GF, Haight GP. Reactions of octacyanomolybdate(IV). III. Infrared and magnetic studies of compounds with divalent first-row transition metals. Inorg Chem 1973;12:3007–8.

[19] Dong W, Sun YQ, Zhu LN, Liao DZ, Jiang ZH, Yan SP, et al. Two different three-dimensional microporous framework structures in $[Mn_2(H_2O)_4\{W(CN)_8\}\cdot 4H_2O]_n$ and $[Mn_2(H_2O)_4\{W(CN)_8\}(OH)\cdot 2H_2O]_n$. New J Chem 2003;27:1760–4.

[20] Willemin S, Larionova J, Clérac R, Donnadieu B, Henner B, Fréderic Le Goff X, et al. Crystal structures and intercalation reactions of three-dimensional coordination polymers $[M(H_2O)_2]_2[Mo(CN)_8]\cdot 4H_2O$ (M = Co, Mn). Eur J Inorg Chem 2003:1866–72.

[21] Leipoldt JG, Box LDC, Cilliers PJ. The preparation of potassium octacyanomolybdate(IV) dihydrate. Z Anorg Allg Chem 1974;407:343–4.

[22] Leipoldt JG, Box LDC, Cilliers PJ. The preparation of potassium octacyanotungstate(IV) dihydrate. Z Anorg Allg Chem 1974;407:350–2.

[23] Ma SL, Ren S, Ma Y, Liao DZ, Yan SP. Three types of heterometallic structural motifs based on $[Mo(CN)_8]^{3-/4-}$ anion and $Mn^{II}$ cation as building blocks. Struct Chem 2009;20:145–54.

[24] Liu BL, Xiao HP, Song Y, You XZ. Two bimetallic W(IV)-Mn(II) complexes based on octacyanometallates: structures and magnetic properties. Sci China Ser B 2009;52:1801–7.

[25] Roquerol F, Roquerol J, Sing K. Adsorption by powders and solids: principles, methodology and applications. London: Academic Press; 1999.

[26] Yang RT. Gas separation by adsorption processes. Boston: Butterworth; 1997.

[27] Kaye SS, Long JR. Hydrogen adsorption in dehydrated variants of the cyano-bridged framework compounds $A_2Zn_3[Fe(CN)_6]_2\cdot xH_2O$ (A = H, Li, Na, K, Rb). Chem Commun 2007:4486–8.

[28] Murray LJ, Dincă M, Long JR. Hydrogen storage in metal-organic frameworks. Chem Soc Rev 2009;38:1294–314.

[29] Kaye SS, Long JR. The role of vacancies in the hydrogen storage properties of Prussian blue analogues. Catal Today 2007;120:311–6.

[30] Rowsell JLC, Yaghi OM. Effects of functionalization, catenation, and variation of the metal oxide and organic linking units on the low-pressure hydrogen adsorption properties of metal-organic frameworks. J Am Chem Soc 2006;128:1304–15.

[31] Chen BL, Zhao XB, Putkham A, Hong KL, Lobkovsky EB, Hurtado EJ, et al. Surface interactions and quantum kinetic molecular sieving for $H_2$ and $D_2$ adsorption on a mixed metal-organic framework material. J Am Chem Soc 2008;130:6411–23.

[32] Culp JT, Natesakhawat S, Smith MR, Bittner E, Matranga C, Bockrath B. Hydrogen storage properties of rigid three-dimensional Hofmann clathrate derivatives: the effects of pore size. J Phys Chem 2008;C112:7079–83.